RSC Advances

ROYAL SOCIETY OF CHEMISTRY

www.rsc.org/advances

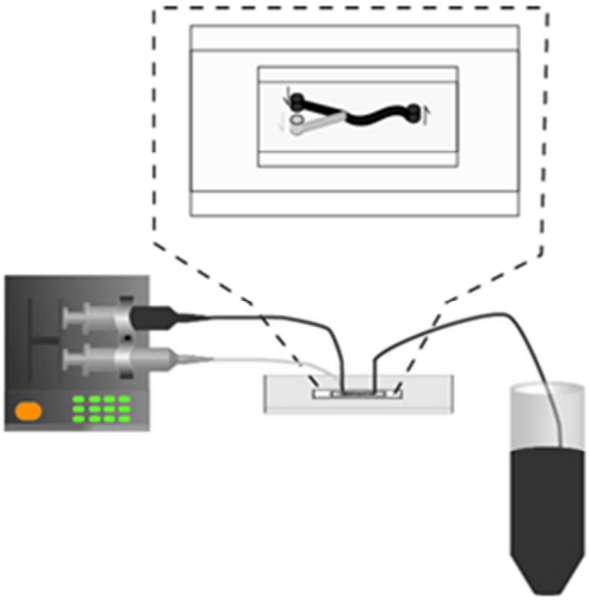

81x78mm (96 x 96 DPI)

Microfluidic-based Controllable Synthesis of Pt Nanocatalysts Supported on Carbon for Fuel Cells

Guangjun Ran, Qiang Fu, and Weilin Xu*

State Key Laboratory of Electroanalytical Chemistry, & Jilin Province Key Laboratory of Low Carbon Chemical Power, Changchun Institute of Applied Chemistry, Chinese Academy of Science, 5625 Renmin Street, Changchun 130022, P.R. China.

*E-mail: weilinxu@ciac.ac.cn

Abstract: A simple custom-made microfluidic reactor is used to synthesize Pt nanoparticles supported on carbon (Pt/C) as electrocatalysts for fuel cells. By varying the flow rate of reactant in the microfluidic reactor, Pt/C catalyst obtained with flow rate of 90 μL/min of substrate was found to be optimal for both anode and cathode electro-catalytic reactions (oxygen reduction reaction (ORR), methanol and formic acid electro-oxidation). An optimal size of Pt nanoparticles was found to be about 2.8 nm. This microfluidic reactor provides a versatile and portable approach to the large-scale synthesis of uniformly-dispersed carbon supported precious metal catalysts with high performance for fuel cells. The preparation is portable, versatile, fast and energy efficient, and can be a general method for the preparation of other supported metal and alloy systems.

Introduction

With the accelerated depletion of fossil fuels and increasing environmental concerns, the development of new alternative energy conversion and storage devices such as fuel cells, supercapacitors, and lithium ion batteries, is very important for solving the present energy crisis.[1] Fuel cells, as an environmentally friendly energy device, have been intensely studied due to their numerous advantages, including high-energy density, high conversion efficiency, quiet operation, and low environmental impacts for various applications.[2-5] At present, tremendous research efforts have been dedicated to the fabrication of efficient fuel cells with high performance. Direct methanol fuel cells or direct formic acid fuel cells, using liquid and renewable methanol or formic acid as fuel, have been considered to be a favorable option in terms of fuel usage and feed strategies and have become a hot topic for portable mobile power.[6-8] Of the noble metal nanomaterials, Pt and Pt-based nanomaterials are still indispensable and the most effective catalysts for fuel cells.[9-14] However, one of the major obstacles for fuel cell commercialization is the high cost and unsustainability of Pt

nanocatalysts used. Thus, advanced Pt-based catalysts with high electrocatalytic activity are highly desirable for the sustainable development of Pt-based catalysts.

The as prepared carbon supported Pt (Pt/C) catalysts could have different morphology, size and catalytic activity due to a wide variety of preparation methods, such as impregnation, ion exchange, chemical vapor deposition, etc.[15-17] Microfluidic synthesis is a micro-reaction technology developed in recent years.[18] Compared with conventional synthetic methods, microfluidic reactor has advantages, such as a higher rate of mass transfer and heat transfer, shorter mixing time, continuous reactions and low reagent consumption, etc.[19] In addition, their narrow reaction channels and customized mixing geometries can provide very precise control over the timing of reagent addition and improved thermal transport properties, two factors that strongly influence the monodispersity of the product nanomaterials.[19-23] Recently, the morphology- and size-controlled synthesis of nanoparticles through microfluidic reactors has caused extensive concern.[24-28] Lee et al.[29] demonstrated a microfluidic approach to synthesize platinum nanoparticles, which were applied to create a hierarchical catalyst by coating the surface of the magnetic silica nanospheres. Baumgard et al.[30] prepared Pt nanoparticles by two-step process using micro-structured devices continuously. The size of Pt-nanoparticles formed inside the microstructures can be controlled by the NaOH/Pt ratio. Luty-Błocho et al.[31] reported a synthesis of platinum nanoparticles and their deposition on the active carbon fibers in one microreactor cycle. In this way, the synthesis of platinum nanoparticles and the deposition on support of carbon fibers were separated. However, the microfluidic reactor-based one-step synthesis of Pt nanocatalysts supported by active carbon (Pt/C) for fuel cells is rarely reported.

In this study, based on a simple and operable custom-made microfluidic reactor, with $NaBH_4$ as a reducing agent, PVP as a stabilizing agent, a microfluidic method was applied to study the effect of flow rates of substrate on the catalytic properties of obtained Pt/C catalysts for fuel cell reactions systematically for the first time. As a result, the narrower Pt nanoparticles size and size distribution can be obtained in the microfluidic reactor.

Materials and methods

Materials. All of the chemicals used were of analytical grade. The carbon black BP 2000 (BP, BET surface area of 1391 m^2/g) was purchased from Asian-Pacific Specialty Chemicals Kuala Lumpur. Methanol (CH_3OH) and formic acid (HCOOH) were purchased from Beijing Chemical Works, China. Hexachloroplatinic acid ($H_2PtCl_6\ 6H_2O$), Polyvinylpyrrolidone (PVP), Sodium borohydride ($NaBH_4$), Sodium hydroxide (NaOH), Potassium hydroxide (KOH) and Nafion solution (5 wt%) were obtained from Aldrich and used as received without further purification. Ultrapure water with the specific resistance of 18.2 MΩ·cm was obtained by reversed osmosis followed by ion-exchange and filtration.

Methods. In a typical synthesis, 20 mL solution (**Sol-A**) containing BP (100 mg), $H_2PtCl_6\ 6H_2O$ (2.56 mM) and PVP (25.6 mM) was prepared first with ultrapure H_2O. Meanwhile, 20 mL $NaBH_4$ solution (**Sol-B**, 51.2 mM) was prepared with ultrapure water. To reduce the hydrolytic rate of the $NaBH_4$ in reaction process, 0.1 M NaOH solution was added to adjust the solution pH to 12. The microfluidic flow reactor with **S**-type mixer is fabricated by sandwiching a piece of double-sided tape with **S**-type channel between two cover slides. The obtained micro-reactor connected with a syringe pump (Harvard Apparatus, USA) via two TYGON polyvinyl tubings (ID 0.2 mm, OD 0.36 mm) as shown in Figure 1. **Sol-A** and S**ol-B** are flowed into the **S**-type mixer and then react; subsequently the reaction is continued in the polyvinyl tubing reaction channel, the final product is collected at the end of the channel with a reagent bottle. The product collected at the end of the channel, separated by centrifugation and washed alternately with large amount of water and ethanol several times, then dried in an oven overnight at 60℃ to yield a final product. By varying the flow rate of the solution, a series of Pt/C catalysts were obtained.

Characterization. X-ray diffraction (XRD) analysis was carried out on Bruker D8-ADVANCE diffractometer with Cu Kα radiation of wavelength λ = 0.15418 nm. Transmission electron microscopy (TEM, TECNAI G^2) was applied to characterize the morphology. X-ray photoelectron spectroscopy (XPS) analysis was used a K-alpha Thermo Scientific spectrometer (X-ray beam with a spot size of 500 μm, monochromatized Al-Kα

line). The analysis of the composition of the catalyst was obtained with an inductively coupled plasma-atomic emission spectrometer (ICP-AES, USA Thermo Jarrell-Ash Corp).

Electrochemical Measurements. The electrochemical experiments were carried out with a CHI 750E system (CH Instrument Co., USA). Rotating ring disk electrode (RRDE) tests were conducted on RRDE-3A apparatus (ALS Company, Japan) with the Glassy Carbon disk, Pt ring electrode (the diameter is 4 mm for disk) and saturated calomel electrode (in saturated KCl, (25 ℃, 4.2 M)) was used as the reference electrode. Fabrication of the working electrodes was done by mixing 5 mg of catalysts, 50.0 μL of a 5 wt % Nafion solution in alcohol, and 950.0 μL of ethanol under ultra-sonication. A 10 μL aliquot of the ink was dropped on the surface of the glassy carbon rotating disk electrode. The activity of Pt/C for oxygen reduction reaction (ORR) was evaluated by cyclic voltammetry (CV) and linear sweep voltammetry (LSV) on glassy carbon electrode. The electrolyte was nitrogen or oxygen-saturated 0.5 M H_2SO_4. The activity of Pt/C for methanol and formic acid electro-oxidation was evaluated by CV on glassy carbon electrode. Fabrication of the working electrodes was done by pasting catalyst inks on a glassy carbon rotating disk electrode (4 mm in diameter). The carbon ink was formed by mixing 5 mg of Pt/C catalysts, 50 μL of 5 wt % Nafion solution in alcohol, and 950.0 μL of ethanol in a plastic vial under ultra-sonication. A 10-μL aliquot of the carbon ink was dropped on the surface of the glassy carbon rotating disk electrode, yielding an approximate catalyst loading of 0.05 mg. The electrolyte was 0.5 M H_2SO_4 or 0.5 M H_2SO_4 + 0.5 M CH_3OH or 0.5 M HCOOH solution; the counter and the reference electrodes were a platinum wire and a SCE electrode, respectively. The potential of the electrode was controlled by an EG&G (model 273) potentiostat/galvanostat system. Cyclic voltammetry was performed from -0.242 V to 0.958 V at 50 mV s^{-1}. The electrochemically active surface areas (EASA, m^2/g_{Pt}) of different catalysts were obtained through CO stripping method. These EASA values were used to normalize the catalytic activity of the catalysts for all these three reactions.

Results & Discussion

In a typical synthesis, 20 mL **Sol-A** containing BP (100 mg), H_2PtCl_6 $6H_2O$ (2.56 mM) and PVP (25.6 mM) and 20 mL **Sol-B** containing 51.2 mM $NaBH_4$ were flowed into the

microfluidic reactor from two independent syringes with the same flow rate. Theoretically, the Pt content on the final Pt/C should be 9.1 wt. % if there is no Pt or carbon loss. By varying the flow rate from 30 μL/min to 150 μL/min gradually, five different Pt/C catalysts were obtained through the microfluidic reactor. The actual Pt contents on these catalysts were obtained by ICP-AES analysis. As shown in Table 1, the Pt contents on Pt/C catalysts are around 9.1 wt.% when the flow rate is lower than 120 μL/min, indicating the complete reduction of Pt; at higher flow rate of 150 μL/min, the final Pt content is about 7.6 wt.%, much lower than the original 9.1 wt.%, indicating the Pt is lost seriously at higher flow rates probably due to the incomplete reduction of $PtCl_6^{2-}$ in the fast flow.

Table 1 Pt contents and size of Pt nanoparticles on Pt/C obtained with different flow rates.

Catalysts samples	Pt content (wt.%)	Average particles size from XRD (nm)	Particle size from TEM (nm)
30μL/min	9.2	3.2	3.3±0.6
60μL/min	9.1	2.9	2.9±0.6
90μL/min	8.9	2.7	2.8±0.5
120μL/min	8.8	2.6	2.7±0.6
150μL/min	7.6	2.4	2.5±0.6

The XRD patterns of different Pt/C catalysts are shown in Fig. S1. All these catalysts exhibit the face centered cubic (*fcc*) structure of Pt with typical diffraction peaks corresponding to Pt (111), Pt (200), Pt (220) and Pt (311).[32] The sizes of Pt crystallite on different Pt/C catalysts were calculated based on the Scherrer equations[33] with the (220) peak of the Pt nanoparticles. Interestingly, the results (Table 1) show a decrease of size with the increase of flow rate of reactant in the microfluidic reactor.[34, 35] The decrease of size could be due to the short growth time of Pt nanoparticles in the microfluidic reactor at high flow rate. The higher peak intensity of (111) facet compared with other facets indicates that the exposed surface on Pt nanoparticle surface is mainly the (111) facets. Furthermore, the Pt/C obtained with flow rate of 90μL/min possesses the highest content of (111) facet. Since Pt(111) facet has been known to be the most active surface compared with others due to its low poisoning rate,[36] the catalyst obtained with flow rate of 90 μL/min may possess the best catalytic performance among these five catalysts due to its highest content of (111) facet.

The morphologies of these five Pt/C catalysts were further characterized with Transmission electron microscopy (TEM). As shown in Fig. 2, TEM images and size distributions of Pt nanoparticles on different catalysts show that the average sizes of Pt nanoparticles on these catalysts are around 3 nm (Table 1). A monotonic decrease of size with the increase of flow rate could be seen clearly, consistent with the XRD results (Table 1 and Fig. S1). Fig. 2 shows that the Pt nanoparticles on all these catalysts are dispersed on the carbon support uniformly. The high-resolution TEM (HRTEM) image shows (Fig. 2f) the Pt nanoparticles on these Pt/C catalysts are crystalline, consistent with the XRD data shown in Fig. S1, but amorphous in shape.

To quantify the heterogeneity of Pt size distribution, we used a heterogeneity index (*h*, in percentage, defined as the full width at half maximum of the distribution divided by the average) to measure the relative spread of values of a parameter from its average, which the larger *h* is the greater heterogeneity the parameter has.[37, 38] The values of *h* for these catalysts were obtained as shown in Fig. 3a. A valley-shape dependence of *h* on flow rates could be observed clearly with minimum located at the flow rate of 90 μL/min, indicating the Pt/C catalyst obtained with flow rate of 90 μL/min has the narrowest particle-size distribution, further implying that the Pt/C catalyst obtained with flow rate of 90 μL/min may possess the best performance among these ones obtained with different flow rates.

In order to confirm the above prediction about the catalytic properties of these catalysts, in the following these catalysts were tested for three different catalytic reactions. Before that, the electrochemically active surface areas (EASA) of these catalysts were obtained through CO stripping since the EASA has been known to be directly related to the catalytic properties of catalysts.[39] Interestingly, Fig. 3b shows that the EASA per gram Pt (m^2/g_{Pt}) on Pt/C could be tuned by varying the flow rate of reactant in the channel: with the flow rate increase, the EASA per gram Pt increases gradually first, then reaches a maximum at the flow rate of 90 μL/min; after that, it goes through a maximum at 90 uL/min at higher flow rates. It probably means that 90 μL/min is the optimal flow rate among these few since it has been known that

the larger the EASA the better the electrocatalyst is.[40]

Firstly, the electrochemical properties of the Pt/C catalysts for ORR were evaluated in O_2-saturated 0.1 M KOH with a scan rate 200 mV s^{-1} (vs. SCE). In order to consider the effect of EASA on the performance of catalysts, the currents (mA cm^{-2}) were all normalized based on the real EASA (m^2) of the catalysts obtained from CO stripping. As shown in Fig. 4a, the oxygen reduction peaks on CV could be clearly observed on these catalysts, while the one with flow rate of 90 μL/min shows the highest peak potential (E_p) for ORR at -0.183 V compared with other catalysts (Fig. 3c). The flow rate dependence of E_p observed here is consistent with the EASA shown in Fig. 3b, confirming that Pt/C with higher EASA usually shows better catalytic performance.[40] Fig. 3d shows the volcano-shape dependence of $\boldsymbol{E_p}$ on size of Pt nanoparticles, indicating an optimal size (~2.8 nm) of Pt corresponds to an optimal catalytic activity, the smaller or larger size of Pt nanoparticles will deteriorate the catalytic activity of catalysts.[41] Linear sweep voltammetry (LSV) results further confirm this point as shown in Figure 4b. It shows the onset potential (E_{on}) on these Pt/C catalysts for ORR varies with flow rates. As depicted in the inset of Fig. 4b, E_{on} of the catalyst shows a volcano-shaped dependence on the flow rate or size of Pt nanoparticles, which is consistent with those shown in Fig. 3, further confirming the flow rate of 90μL/min is optimal. For comparison, the performance of commercial Pt/C is also shown in Fig. 4; its performance is almost the same as that of the optimal catalyst obtained with flow rate of 90μL/min.

To understand the electron transfer kinetics of the optimal catalyst obtained with flow rate of 90 μL/min for ORR, we studied its ORR reaction kinetics on a rotating ring-disk electrode. The disk currents of LSV with various rotation rates were given in Fig. S2a. Koutecky-Levich equation[42] was used for analyzing the transferred electron number (***n***) during the ORR with disk currents.

$$\frac{1}{j} = \frac{1}{j_L} + \frac{1}{j_K} = \frac{1}{B\omega^{1/2}} + \frac{1}{j_K}$$

in which

$$B = \frac{0.2nFC_{O_2}D_{O_2}^{2/3}}{V^{1/6}}$$

Where j is the overall current density, j_L is the diffusion-limiting current density, j_K is the kinetic current density, ω is the rotation speed, F is the Faraday constant (96485 C mol^{-1}), C_{O_2} is the bulk concentration of O_2 (1.2×10^{-6} mol cm^{-3}), D_{O_2} is the diffusion coefficient of O_2 (1.9×10^{-5} cm^2 s^{-1}), v is the kinematics viscosity of the electrolyte (0.01 cm^2 s^{-1}) and n is the transferred electron numbers in the ORR. In the j^{-1} versus $\omega^{-1/2}$ plot, the slope is *1/B*. As shown in Fig. S2b (at -0.6 V vs. SCE), the number of electrons transferred (*n*) was calculated from the slope of the Koutecky–Levich plots, by using the above parameters and Koutecky-Levich equation. The number of electrons obtained from the slope is 4.0 for the optimal catalyst, indicating that the ORR is a four-electron process that completely reduces the O_2 to H_2O on the optimal catalyst.

To further consider the potential effect on the catalytic activity of optimal catalyst, we analyzed the ring-disk currents on the catalyst at different potential. As shown in Fig. S2c,d, the optimal Pt/C can greatly inhibit the two electron (or H_2O_2) pathway and make water the main product (four-electron pathway) in the whole wide potential window, indicating a little bit better performance than that of commercial Pt/C.

In order to further confirm the versatility of the prepared catalysts, these catalysts were also tested as electrocatalysts for both methanol and formic acid electro-oxidation. As shown in Fig. 5a for methanol electro-oxidation in 0.5 M H_2SO_4 + 0.5 M CH_3OH, all these prepared catalysts showed obvious methanol oxidation peaks appeared in both the forward and reverse scans. The peak current densities of methanol oxidation are in the order of 90 μL/min > 120 μL/min > 60 μL/min > 30 μL/min > 150 μL/min, which is consistent with as that shown in Fig. 3 or Fig. 4b, further confirming that the catalyst obtained with flow rate of 90 μL/min is still the optimal one for methanol electro-oxidation. The ratio of the forward anodic peak current density (I_f) to the reverse anodic peak current density (I_b), I_f/I_b, can be used to describe the catalyst tolerance to carbonaceous species accumulation. Low I_f/I_b ratio indicates poor oxidation of methanol to carbon dioxide during the anodic scan and excessive accumulation of carbonaceous residues on the catalyst surface.[43] High I_f/I_b ratio shows the converse case. The large value (1.47) of I_f/I_b on optimal catalyst obtained with flow rate of 90 μL/min (*vs.* 0.84 on commercial Pt/C) implicates that methanol molecules can be more effectively

oxidized to CO_2 on the optimal catalyst during the forward potential scan, generating relatively less poisoning species as compared to commercial Pt/C.

Similarly, Fig. 5b shows the catalyst obtained with flow rate of 90 μL/min is also the best one for formic acid oxidation compared with others. The reaction on this catalyst commences in the hydrogen region and proceeds slowly during the forward scan. This corresponds to formic acid oxidation through the dehydrogenation path, but the coverage by CO simultaneously continues to grow and causes only relatively small shoulder peak currents at about 0.28 V.[44, 45] At higher potentials, the current further increases and reaches another peak at 0.67 V. The peak could be attributed to the oxidation of adsorbed CO and formic acid on available active sites recovered by CO removal. [45, 46] In the reversing the potential scan, the surface remains inactive until partial reduction of the irreversibly formed surface oxides. One huge anodic peak near 0.29 V is observed, and is due to the oxidation of formic acid after reduction of Pt oxides.[47] As compared to commercial Pt/C, the formic acid oxidation shifts to lower potential and this indicates superior catalytic activity.[44]

Table 2. Binding energy (B.E.) of Pt species observed from XPS of catalyst of 90 and 150 μL/min

Catalysts samples	B. E. of Pt(0)/eV	B. E. of Pt(Ⅱ)/eV
90 μL/min	71.3/ 74.4	72.4/75.7
150 μL/min	71.4/74.5	72.4/75.7

In order to chemically understand why the optimal Pt/C obtained with flow rate of 90 μL/min possesses the highest catalytic performance compared with others, XPS was employed to analyze the valence state of Pt. The XPS spectrum of Pt 4f in the optimal catalyst Pt/C obtained with flow rate of 90μL/min has been de-convoluted and shown in Fig. 6a. The Pt 4f region displays two doublets from the spin-orbital splitting of the $4f_{7/2}$ and $4f_{5/2}$ states. The most intense doublets (71.3 and 74.4 eV) could be due to metallic Pt (0). The second set of doublets (72.4 and 75.7 eV) could be assigned to the Pt(II) in PtO.[7, 41] Similarly, de-convolution of the XPS has been carried out for the catalyst obtained with flow rate of 150 μL/min (Fig. 6b) which possesses the lowest catalytic activity and the presence of Pt(0) and

Pt(II) species are also confirmed by the peaks shown in Fig. 6b. As shown in Table 2, the binding energies of Pt (0) and Pt (II) show almost no difference between different flow rates, indicating the activity difference was not induced by the different chemical states of Pt. According to the TEM images shown in Fig. 2, the activity difference could be mainly attributed to the difference in morphology or size of Pt nanoparticles induced by the different flow rate.[48, 49]

By now, Pt/C catalysts have been extensively prepared with different methods with the control of size, morphology, or density of Pt nanoparticle supported on carbon-based surfaces.[4-17, 23] However, most of these preparations are based on traditional method without continuity.[4,5,8,14,23] With the microfluidic-based method presented here, besides the fine tuning of the size and morphology of Pt nanoparticles supported on carbon, the Pt/C catalyst with optimal performance could be produced continuously with an optimal flow rate in one step simply.

Conclusions

In a summary, a novel and simple microfluidic reactor is used to prepare carbon-supported Pt catalysts for ORR, methanol and formic acid electro-oxidation for fuel cells. By varying the flow rate of reactant in the microfluidic reactor, Pt/C catalyst obtained with flow rate of 90 μL/min was found to be optimal for all these three electro-catalytic reactions. An optimal size of Pt nanoparticles was found to be about 2.8 nm. We anticipate that this microfluidic reactor will provide a blueprint for a versatile and portable approach to the large-scale synthesis of uniformly-dispersed carbon supported precious metal catalysts with high performance for fuel cells. The preparation is portable, versatile, fast and energy efficient, and can be used as a general method for the preparation of other supported metal and alloy systems.

Acknowledgment. This work was funded by the National Basic Research Program of China (973 Program, 2012CB932800 and 2014CB932700), National Natural Science Foundation of China (21273220 and 21422307), and “the Recruitment Program of Global youth Experts” of China.

References

1. H. Liu, C. Song, L. Zhang, J. Zhang, H. Wang and D. P. Wilkinson, *Journal of Power Sources*, 2006, **155**, 95-110.
2. L. Zhang, J. Niu, M. Li and Z. Xia, *The Journal of Physical Chemistry C*, 2014, **118**, 3545-3553.
3. Y. Zhang, K. Fugane, T. Mori, L. Niu and J. Ye, *Journal of Materials Chemistry*, 2012, **22**, 6575-6580.
4. J. C. Claussen, A. Kumar, D. B. Jaroch, M. H. Khawaja, A. B. Hibbard, D. M. Porterfield and T. S. Fisher, *Advanced Functional Materials*, 2012, **22**, 3399-3405.
5. D.-D. La, C. K. Kim, T. S. Jun, Y. Jung, G. H. Seong, J. Choo and Y. S. Kim, *Sensors and Actuators B: Chemical*, 2011, **155**, 191-198.
6. Y.-W. Rhee, S. Y. Ha and R. I. Masel, *Journal of Power Sources*, 2003, **117**, 35-38.
7. X. Wang, J.-M. Hu and I. Hsing, *Journal of Electroanalytical Chemistry*, 2004, **562**, 73-80.
8. Y. Mu, H. Liang, J. Hu, L. Jiang and L. Wan, *The Journal of Physical Chemistry B*, 2005, **109**, 22212-22216.
9. G. Camara, R. De Lima and T. Iwasita, *Journal of Electroanalytical Chemistry*, 2005, **585**, 128-131.
10. M. Nie, H. Tang, Z. Wei, S. P. Jiang and P. K. Shen, *Electrochemistry Communications*, 2007, **9**, 2375-2379.
11. E. Antolini, F. Colmati and E. Gonzalez, *Journal of power sources*, 2009, **193**, 555-561.
12. E. Lee, I.-S. Park and A. Manthiram, *The Journal of Physical Chemistry C*, 2010, **114**, 10634-10640.
13. J. Datta, A. Dutta and S. Mukherjee, *The Journal of Physical Chemistry C*, 2011, **115**, 15324-15334.
14. B. H. Morrow and A. Striolo, *Nanotechnology*, 2008, **19**, 195711.
15. A. R. Tao, S. Habas and P. Yang, *Small*, 2008, **4**, 310-325.
16. S.-Y. Lee and R. Aris, *Catalysis Reviews Science and Engineering*, 1985, **27**, 207-340.
17. Z. Yan, M. Wang, Y. Lu, R. Liu and J. Zhao, *Journal of Solid State Electrochemistry*, 2014, **18**, 1087-1097.
18. P. N. Nge, C. I. Rogers and A. T. Woolley, *Chemical reviews*, 2013, **113**, 2550-2583.
19. J. Puigmartí-Luis, *Chemical Society reviews*, 2014, **43**, 2253-2271.
20. P. R. Makgwane and S. S. Ray, *Journal of nanoscience and nanotechnology*, 2014, **14**, 1338-1363.
21. S. E. Lohse, J. R. Eller, S. T. Sivapalan, M. R. Plews and C. J. Murphy, *ACS nano*, 2013, **7**, 4135-4150.
22. C. V. Navin, K. S. Krishna, C. S. Theegala and C. S. Kumar, *Nanotechnology Reviews*, 2014, **3**, 39-63.
23. J. C. Claussen, M. A. Daniele, J. Geder, M. Pruessner, A. J. Mäkinen, B. J. Melde, M. Twigg, J. M. Verbarg and I. L. Medintz, *ACS applied materials & interfaces*, 2014, **6**, 17837-17847.
24. A. M. Nightingale and J. C. deMello, *Advanced materials*, 2013, **25**, 1813-1821.
25. R. C. Wootton, *Nature*, 2012, **483**, 43-44.
26. Y. Song, J. Hormes and C. S. Kumar, *Small*, 2008, **4**, 698-711.
27. K. S. Krishna, Y. Li, S. Li and C. S. Kumar, *Advanced drug delivery reviews*, 2013, **65**, 1470-1495.
28. C.-X. Zhao, L. He, S. Z. Qiao and A. P. Middelberg, *Chemical Engineering Science*, 2011, **66**, 1463-1479.
29. S.-K. Lee, X. Liu, V. S. Cabeza and K. F. Jensen, *Lab on a chip*, 2012, **12**, 4080-4084.
30. J. Baumgard, A.-M. Vogt, U. Kragl, K. Jähnisch and N. Steinfeldt, *Chemical Engineering Journal*, 2013, **227**, 137-144.
31. M. Luty-Błocho, M. Wojnicki, K. Pacławski and K. Fitzner, *Chemical Engineering Journal*, 2013, **226**, 46-51.
32. J. Xu, T. Zhao and Z. Liang, *Journal of Power Sources*, 2008, **185**, 857-861.
33. A. Pozio, M. De Francesco, A. Cemmi, F. Cardellini and L. Giorgi, *Journal of power sources*, 2002, **105**, 13-19.
34. T. Teranishi, M. Hosoe, T. Tanaka and M. Miyake, *The Journal of Physical Chemistry B*, 1999, **103**, 3818-3827.
35. W. Li, W. Zhou, H. Li, Z. Zhou, B. Zhou, G. Sun and Q. Xin, *Electrochimica Acta*, 2004, **49**, 1045-1055.
36. J. Solla-Gullon, F. J. Vidal-Iglesias, A. Lopez-Cudero, E. Garnier, J. M. Feliu and A. Aldaz, *Physical Chemistry Chemical Physics*, 2008, **10**, 3689-3698.

37. K. S. Han, G. Liu, X. Zhou, R. E. Medina and P. Chen, *Nano Lett.*, 2012, **12**, 1253-1259.
38. W. Xu, J. S. Kong and P. Chen, *Phy. Chem. Chem. Phy.*, 2009, **11**, 2767-2778.
39. T. Vidaković, M. Christov and K. Sundmacher, *Electrochimica Acta*, 2007, **52**, 5606-5613.
40. X. Huang, E. Zhu, Y. Chen, Y. Li, C. Y. Chiu, Y. Xu, Z. Lin, X. Duan and Y. Huang, *Advanced materials*, 2013, **25**, 2974-2979.
41. J. Guo, T. Zhao, J. Prabhuram and C. Wong, *Electrochimica Acta*, 2005, **50**, 1973-1983.
42. S. Treimer, A. Tang and D. C. Johnson, *Electroanalysis*, 2002, **14**, 165-171.
43. Z. Liu, X. Y. Ling, X. Su and J. Y. Lee, *The Journal of Physical Chemistry B*, 2004, **108**, 8234-8240.
44. Z. Liu, L. Hong, M. P. Tham, T. H. Lim and H. Jiang, *Journal of Power Sources*, 2006, **161**, 831-835.
45. Y. Lu and W. Chen, *The Journal of Physical Chemistry C*, 2010, **114**, 21190-21200.
46. V. M. Jovanović, D. Tripković, A. Tripković, A. Kowal and J. Stoch, *Electrochemistry communications*, 2005, **7**, 1039-1044.
47. M. Osawa, K. i. Komatsu, G. Samjeské, T. Uchida, T. Ikeshoji, A. Cuesta and C. Gutiérrez, *Angewandte Chemie International Edition*, 2011, **50**, 1159-1163.
48. A. E. Souza, S. R. Teixeira, C. Morilla-Santos, W. H. Schreiner, P. N. Lisboa Filhod and E. Longoe, *J. Mater. Chem. C* 2014, **2**, 7056-7070.
49. D. Li, C. Wang, D. S. Strmcnik, D. V. Tripkovic, X. Sun, Y. Kang, M. Chi, J. D. Snyder, D. v. d. Vliet, Y. Tsai, V. R. Stamenkovic, S. Sun and N. M. Markovic, *Energy Environ. Sci.*, 2014, **7**, 4061-4069.

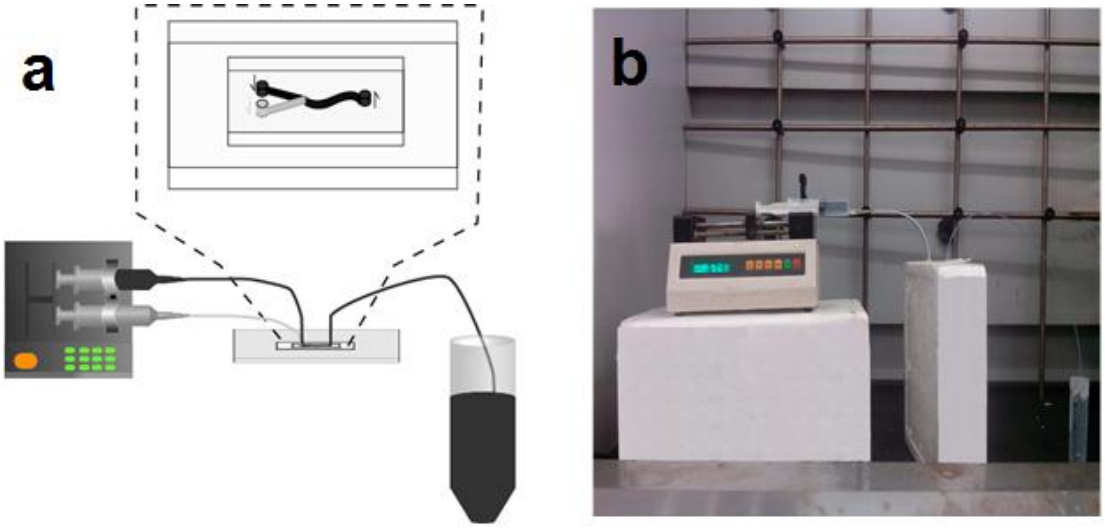

Figure 1. (a) Schematic diagram of the microfluidic reactor system; (b) The real image for the setup of the microfluidic reactor system.

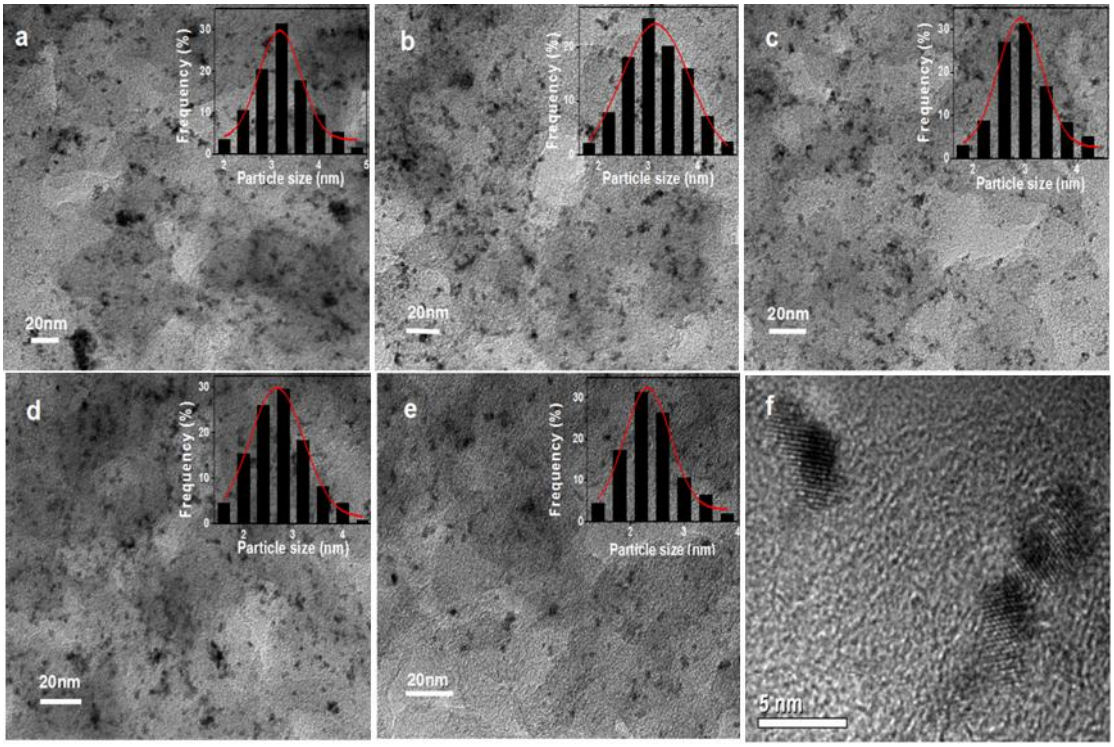

Figure 2. Typical TEM images of Pt/C catalysts obtained with different flow rates: (a) 30 μL/min, d=3.3±0.6 nm (b) 60 μL/min, d=2.9±0.6 nm (c) 90 μL/min, d=2.8±0.5 nm (d) 120 μL/min, d=2.7±0.6 nm and (e) 150 μL/min, d=2.5±0.6 nm. The insets are the corresponding particle size distributions. (f) HRTEM image of Pt nanoparticles on Pt/C catalyst with flow rate of 90 μL/min.

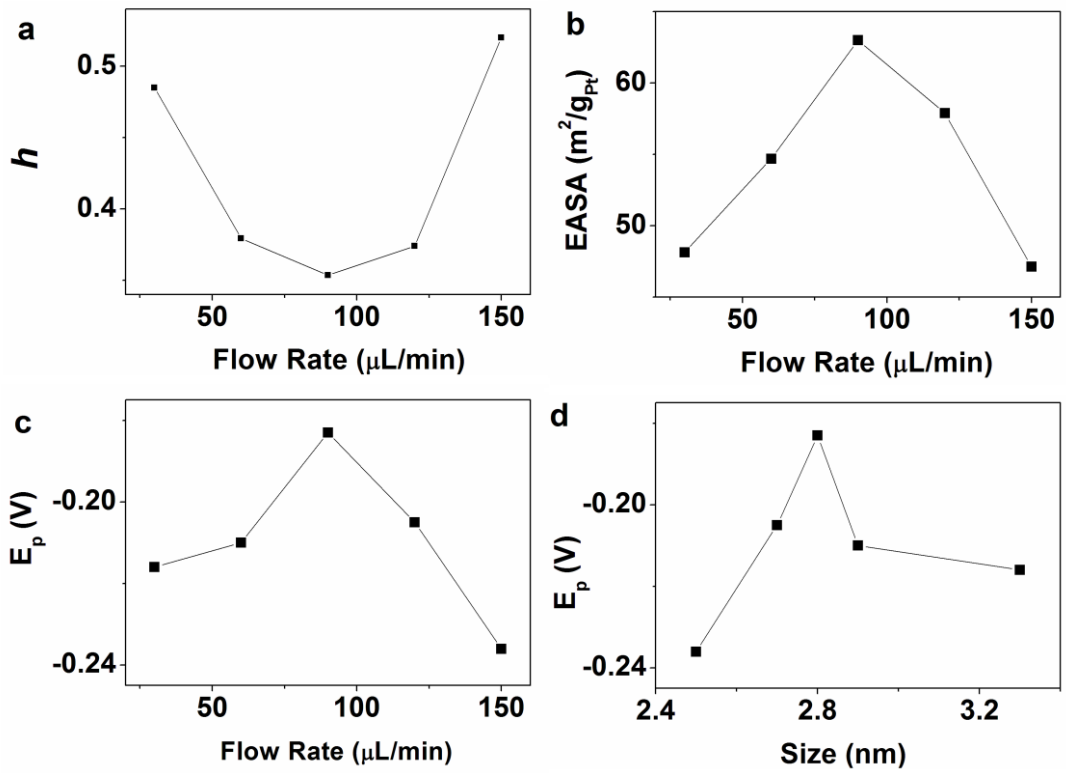

Figure 3. The flow rate dependence of ***h*** (a), ***EASA*** (b) and E_p (c) on Pt/C catalysts obtained with different flow rate. (d) The size dependence of E_p on different Pt/C.

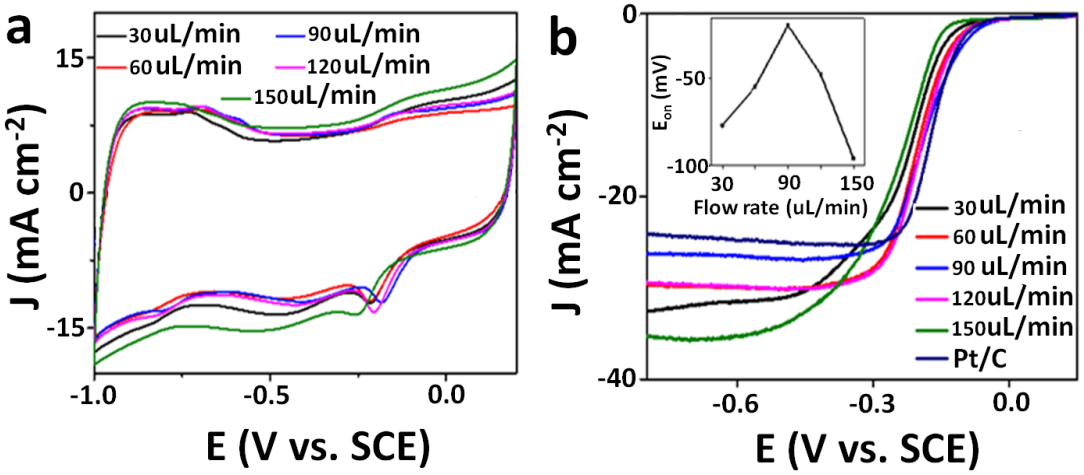

Figure 4. (a) CVs for Pt/C catalysts with different flow rates and commercial Pt/C in O_2-saturated 0.1 M KOH, scan rate 50 mV s^{-1}; (b) polarization curves of different Pt/C catalysts (including commercial Pt/C) for ORR in O_2-saturated 0.1 M KOH, scan rate 50 mV s^{-1}, and the electrode rotation speed was 1,600 rpm, the inset is Volcano-shaped dependences of E_{on} on catalysts of different flow rates.

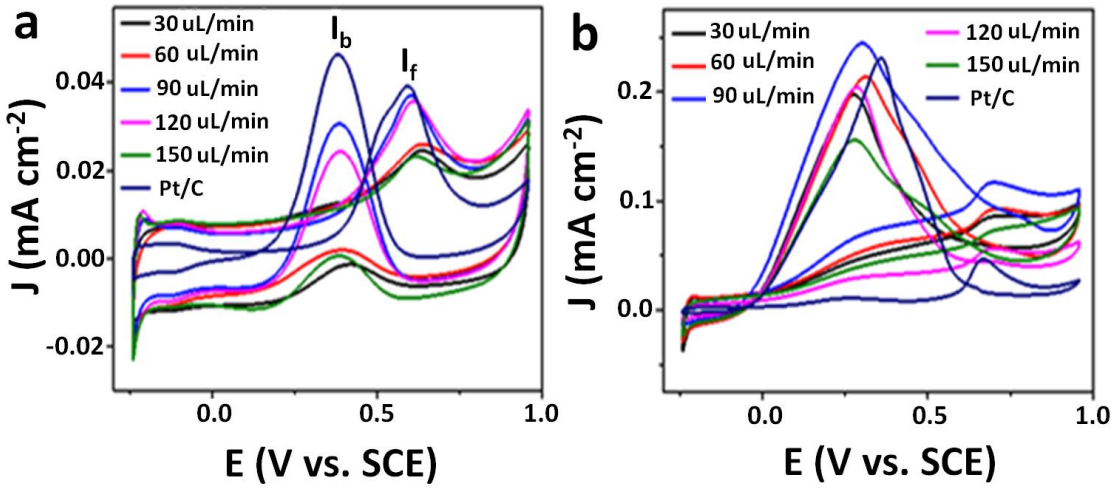

Figure 5. (a) Cyclic voltammograms of Pt/C catalysts with different flow rates in 0.5 M H_2SO_4 + 0.5 M CH_3OH; (b) Cyclic voltammograms of Pt/C catalysts with different flow rates in 0.5 M H_2SO_4 + 0.5 M HCOOH.

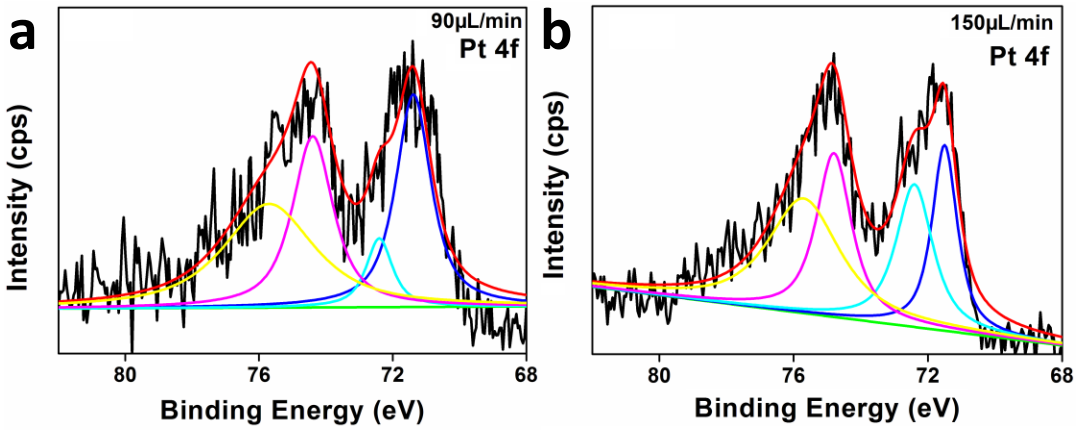

Figure 6. Pt 4f regions of the XPS spectrum: (a) catalyst of 90 μL/min, (b) catalyst of 150 μL/min.

TOC

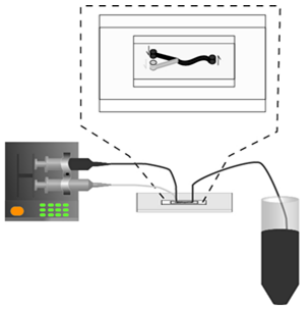

A simple custom-made microfluidic reactor is used to synthesize Pt nanoparticles supported on carbon continuously as electrocatalysts for fuel cells